Research Article Vol. 1, No. 5 / 15 May 2022 / Optics Continuum 1015
OPTICS CONTINUUM

Third harmonic generation enhancement from silicon-based multilayer guided mode resonance structures under a conical mounting condition

SRUTI MENON, K. M. JYOTHSNA, RABINDRA BISWAS, ASISH PROSAD, A. S. LAL KRISHNA, AND VARUN RAGHUNATHAN*

Electrical Communication Engineering Department, Indian Institute of Science, Bangalore 560012, India
varunr@iisc.ac.in

Abstract: We experimentally demonstrate more than four-orders of magnitude enhancement in third harmonic generation from an amorphous silicon layer as thin as 10 nm deposited above silicon nitride guided mode resonance (GMR) structures under a conical mounting condition using a rectangular aperture as a pupil plane mask for the fundamental excitation. The multilayer GMR structure studied here consists of shallow etched one-dimensional silicon dioxide gratings with a silicon nitride intermediate layer and an amorphous silicon nonlinear medium. Under conical mounting, by restricting the fundamental excitation angles along the grating vector direction, while retaining the angles supported by the objective lens along the grating lines, the resonances are made angle insensitive. The forward detected THG enhancement increases from 2860 in the absence of any pupil plane mask, with a uniform fundamental excitation angular span of 2.3° to 4740 and 1.7×10^4 in the presence of rectangular apertures that selectively reduce the excitation angular span along the grating vector direction to 0.86° and 0.43°, respectively. Conical mounting using rectangular aperture pupil masks to engineer the fundamental excitation is a promising approach to enhance nonlinear optical processes from angle sensitive GMR structures.

1. Introduction

Guided mode resonant (GMR) structures and resonant metasurfaces with one- and two-dimensional sub-wavelength dielectric elements achieve diverse spectral characteristics with resonant field enhancement which finds applications in optical filtering [1], refractive index sensing [2,3], fluorescence [4,5] and, nonlinear optical studies [6–12]. The interaction of the incident light with the periodic grating structure results in the coupling of guided modes within the high effective index guiding layer followed by interference of the out-coupled radiation with the as reflected or transmitted light, giving rise to interesting spectral characteristics observed in the GMR structures [13,14]. High index contrast fully etched dielectric grating structures [14,15] and high-quality factor silicon-based resonant metasurfaces [16–19] exhibit angle insensitive spectral response due to the excitation of almost constant resonant mode field profile as a function of varying angle of incidence. Such structures have been used for nonlinear optical enhancement studies [10,16,19–21]. In contrast, the resonances observed in partially etched zero-contrast grating structures [22] and low/ medium index contrast GMR structures [23] are found to be highly angle sensitive. The angle sensitivity of low index contrast GMR structures is especially undesirable when using focused Gaussian beam incidence on finite extent structures, as this lowers the contrast and quality factor of the resonances [24,25]. Low/medium-index contrast GMR structures made of silicon nitride [6,26] and polymer-based [7] sub-wavelength gratings have been utilized for enhancing harmonic generation processes, often requiring angle selective, low divergence excitation of large area structures. Low index nanostructures are a promising platform for integration of emerging two-dimensional materials for strain engineering and quantum light emission [27]. The low refractive index materials such as silicon dioxide and silicon nitride offer

#453943 https://doi.org/10.1364/OPTCON.453943
Journal © 2022 Received 17 Jan 2022; revised 23 Mar 2022; accepted 4 Apr 2022; published 25 Apr 2022

OPTICS CONTINUUM

the added benefit of negligible absorption losses in the visible and near infrared wavelength range spanning both the fundamental and harmonic wavelengths, due to their wider bandgaps. This is often not possible in high-index contrast silicon or germanium based metasurface platforms. Though there are previous reports of angle tolerant resonant metasurfaces for nonlinear optical enhancement studies [19], there are many implementations of angle sensitive resonant surface relief structures that are useful for nonlinear optical studies [6,7]. In this context, conical mounting of one-dimensional GMR structures with the plane of incidence oriented along the grating lines is beneficial and known to improve angular tolerance [28,29] for linear applications. Figure 1(a) and (b) shows the top view schematic of GMR grating structures with the incident and diffracted wave-vectors shown for full-classical and full-conical mounting condition respectively [29,30]. The full-classical (full-conical) mounting condition refers to the plane-of-incidence aligned perpendicular (parallel) to the grating lines. We distinguish between the full-conical (full-classical) mounting used in design studies from the realistic conical (classical) mounting used in experiments due to the non-zero angular spread along the perpendicular directions. In the case of conical mounting, the diffracted wave-vectors which are responsible for GMR remain independent of the angle-of-incidence along the grating lines, resulting in reduced angular sensitivity of the excited GMR. Conical mounting condition has been utilized previously in GMR based optical filters [29–33]. Resonantly enhanced fluorescence imaging using a cylindrical lens before the objective lens to focus the light into a pencil beam at the back focal plane has also been utilized to selectively excite along one grating axis [34]. To the best of our knowledge, conical mounting condition has not been utilized in nonlinear optical studies in resonant grating structures. Nonlinear optical enhancement studies in such structures benefit from the angular insensitivity of the resonances under conical mounting, resulting in efficient excitation of the fundamental resonant fields across a wide excitation angular span.

In this work, we demonstrate more than four-orders of magnitude enhancement in third harmonic generation (THG) from angle-sensitive multilayer GMR structures composed of amorphous silicon (a-Si) layer deposited over silicon nitride (SiN) on silicon dioxide (SiO_2) sub-wavelength gratings using rectangular pupil masks to implement conical mounting condition. The rectangular aperture placed near the back focal plane of the objective lens with the long axis aligned parallel to the grating lines results in reduced illumination angle along the grating vector direction. The forward detected THG enhancements from the a-Si layer as thin as 10 nm increases from 2860 in the absence of any pupil plane mask, with fundamental excitation angle spanning 0–2.3° to 4740 (1.7×10^4) in the presence of rectangular apertures that selectively reduce the excitation angle along the grating vector direction to 0.86° (0.43°) respectively. The improved THG enhancement observed under conical mounting when compared to classical mounting due to efficient excitation of fundamental resonant field is validated using both nonlinear wave propagation simulations and experimental studies. The experimental demonstration in this paper is focused on a particular implementation of multilayer GMR structure with large angular sensitivity. Nonetheless, the technique presented in this work is general and is a promising approach to enhance nonlinear optical processes from any angle sensitive GMR structure or resonant metasurface.

OPTICS CONTINUUM

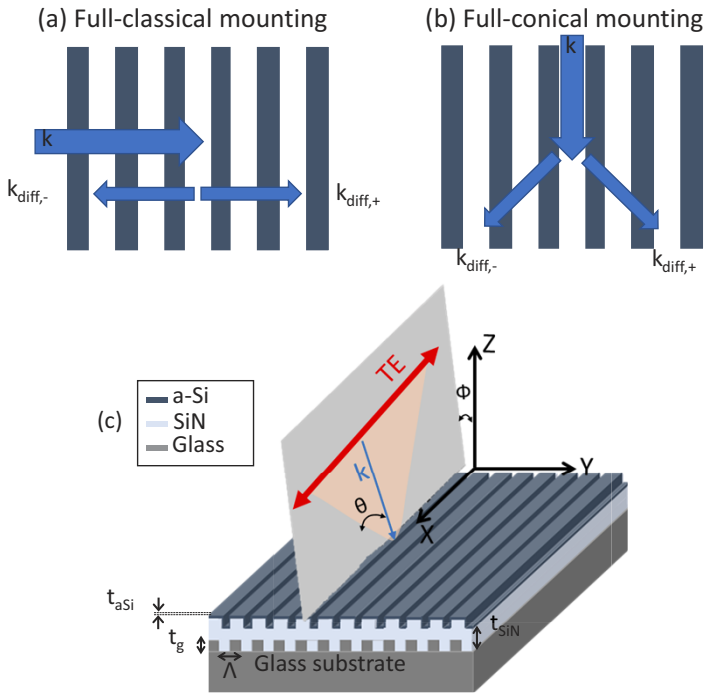

Fig. 1. Schematic top-view representation of: (a) full-classical mounting and (b) full-conical mounting condition with the incident and diffracted wave vector directions indicated with respect to the grating orientation, (c) Schematic of the GMR structure shown with full-conical incidence condition and the co-ordinate axes.

2. Linear and nonlinear optical simulation studies

A schematic of the multi-layer GMR structure used here for THG studies is shown in Fig. 1(c). The structure consists of shallow etched SiO_2 gratings on a glass substrate with intermediate SiN layer followed by a thin a-Si layer. The choice of this multilayer stack with increasing refractive index helps in engineering the resonant field profiles with the SiN layer/SiO_2 grating structure defining the quality factor of the resonances and the ultrathin a-Si overlayer acting as the nonlinear optical medium. The input light polarization is fixed here as transverse electric (TE) oriented along the grating lines. To understand the angular sensitivity of the GMR resonances, we first study the incidence angle dependence of the linear transmission spectra using Stanford Stratified Structure Solver (S4), rigorous coupled-wave analysis (RCWA) solver under plane-wave incidence condition [35]. The multilayer GMR structure studied here comprises of a shallow etched SiO_2 grating of height, $t_g = 70$ nm on a glass substrate with SiN layer, $t_{SiN} = 160$ nm and a-Si layer, $t_{aSi} = 10$ nm. The pitch and duty-cycle are chosen as: $\Lambda = 1050$ nm and 50% respectively. The above dimensions are chosen to ensure good overlap of the resonant electric field within the a-Si layer, as discussed in our previous report on resonant mode field engineering in silicon-based multilayer GMR structures in Ref. [25]. Figures 2(a) and (b) show the transmission spectra contour maps as a function of varying angle-of-incidence (AOI) under full-classical and conical mounting conditions respectively, for plane wave incidence. At normal incidence, the SiN/SiO_2 low-index GMR structure results in narrow linewidth resonance at 1545 nm (not shown here), which red-shifts to 1597 nm in the presence of the a-Si layer. For classical mounting, the resonance is found to split into two distinct branches which move apart from the normal incidence resonance [1,32]. In contrast, for conical mounting condition, the resonances are found to be

OPTICS CONTINUUM

angle insensitive with a small blue-shift of the single prominent resonance dip. The observed blue shift for conical mounting is attributed to the increase in the guided-mode wave-vector with increasing AOI [29]. The wavelength shift of the resonance with increasing AOI is quantified as ~216 nm and 20 nm for increase in AOI of up to 15° for the full-classical and conical mounting conditions respectively, underscoring the angular sensitivity of the low-index contrast multilayer GMR structures.

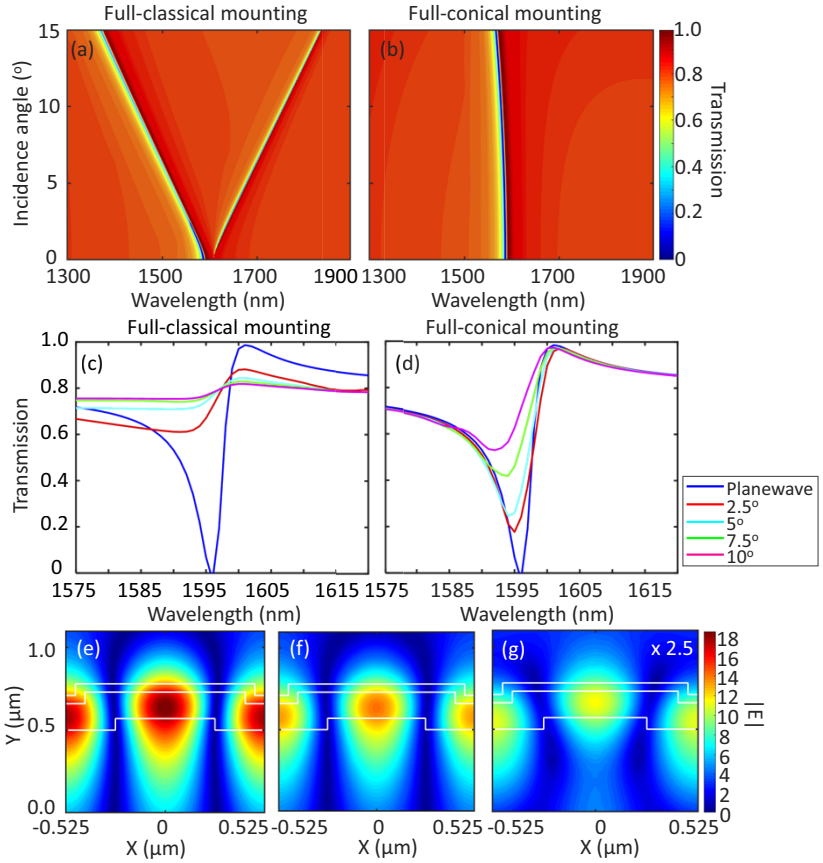

Fig. 2. Transmission contour considering planewave excitation as a function of incidence angle for: (a) full-classical and (b) full-conical mounting condition. Transmission spectra considering 2D Gaussian illumination for varying angular spread for: (c) full-classical and (d) full-conical mounting condition. Corresponding electric field profiles are shown at the respective resonance wavelengths for: (e) planewave excitation, (f) full-conical and (g) full-classical mounting with angular spread of 2.5°. The color-bar in (e-g) represents the normalized electric field values.

Figure 2(c) and (d) shows the simulated transmission spectra under Gaussian beam excitation of grating structures with finite spatial extent. These simulations were performed using COMSOL Multi-physics wave-optics simulations, solving for the linear wave propagation equation and collecting the transmitted light [36]. The excitation considered is a 2D Gaussian beam with varying angular divergence propagating along the z-axis and focused along the y and x axis, with uniform illumination along the perpendicular axis for modeling full-classical and full-conical mounting conditions respectively. The GMR contrast reduces and spectral width increases significantly with increase in the angular spread of the incident beam for full-classical mounting case when compared to the full-conical mounting condition. The corresponding cross-sectional

OPTICS CONTINUUM

electric field profiles for plane-wave incidence, full-conical and full-classical mounting with angular span of 2.5° are shown in Figs. 2(e)–(g) respectively. It is observed that the electric field amplitude inside the GMR structure for the full-conical mounting case closely resembles the ideal plane-wave excited resonant mode profile with a slight reduction in field amplitude (~1.3x). In contrast, the full-classical mounting case results in a significant reduction in the field strength (~3.5x) when compared to the full-conical mounting case. This enhancement in fundamental electric-field for the conical mounted excitation leads to an enhancement of the on-resonance nonlinear optical process, as discussed below. The evanescent field percentage that overlaps with the a-Si nonlinear optical medium is estimated as ~22% [25].

The THG signal spectra from the multilayer GMR structures is obtained under fundamental excitation with Gaussian beams of varying angular divergence. The nonlinear-wave propagation equation used to calculate the THG field strength, $\vec{\boldsymbol{E}}(3\omega)$ in the far field with the nonlinear polarization, $\overrightarrow{\boldsymbol{P}^{(3)}}(3\omega)$ acting as the driving term is given by [37]:

$$\nabla \times \mu_r{}^{-1}(\nabla \times \vec{\boldsymbol{E}}(3\omega)) - k_0^2\left(\epsilon_r(3\omega) - j\frac{\sigma}{\omega\epsilon_0}\vec{\boldsymbol{E}}(3\omega)\right) = \omega^2\mu_0.\overrightarrow{\boldsymbol{P}^{(3)}}(3\omega) \tag{1}$$

Here, the significant THG nonlinear polarization term for TE-polarized fundamental excitation is along the x-axis and is given as a function of the x-polarized fundamental field, $E_x(\omega)$ as:

$$P_x^{(3)}(3\omega) = \chi^{(3)}_{xxxx}.E_x(\omega)^3 \tag{2}$$

This cubic dependence of THG nonlinear polarization on the resonant field is the origin of THG enhancement from the guided-mode resonant structure. It is assumed that the crystallographic x-axis is aligned with the lab co-ordinate x-axis (shown in Fig. 1(a)). The fundamental Gaussian excitation with varying divergence angles propagating along the optical axis are considered here, as described in the linear transmission studies above. The THG electric fields are calculated for different excitation angular spread on- and off- the GMR structure by numerically solving Eq. (1) using COMSOL wave-optics module. Figure 3(a-c) shows the forward collected THG signal power spectra obtained by varying the fundamental excitation wavelength around the GMR resonance for full-classical, conical and off the GMR structures respectively. The off-grating excited THG spectra are identical for both classical and conical mounting with the observed increase in THG signal with increasing angular span of the fundamental excitation, as seen in Fig. 3(c). This is attributed to the increasing optical intensity at the fundamental excitation, resulting in increasing THG signal strength. Similar trend is also observed for the full-conical mounting case as well up to 5° divergence angle in Fig. 3(b) due to decreased angle sensitivity of the gratings. In contrast, for full-classical mounting condition, the THG spectra increases in strength with reducing excitation angular range of the incident fundamental, as seen in Fig. 3(a). It is found that the full-conical mounting condition exhibits more than 500-times higher THG signal when compared to full-classical case. This is attributed to the optimal excitation of the GMR across a wider angular span when using conical mounting condition.

Figure 3(d) shows the THG enhancement spectra obtained by taking the ratio of the THG signals on- and off- the GMR structure after suitably weighing and integrating the THG spectrum by the fundamental pulsed excitation source spectrum used in the experiments (~30 nm full-width half-maximum, Gaussian spectral profile). The THG enhancement for the full-conical mounting can be two to three-orders of magnitude higher than the full-classical case, with different trends observed as a function of varying angular spread of the incident Gaussian beam. The multifold increase in THG enhancement for conical mounting is attributed to the reduced angular sensitivity of the resonance, allowing efficient excitation of the resonance across the excitation angular range. For zero angular spread, which is equivalent to a plane-wave excitation, the THG enhancement is identical for both mounting conditions. In summary, the choice of the excitation angular range

OPTICS CONTINUUM

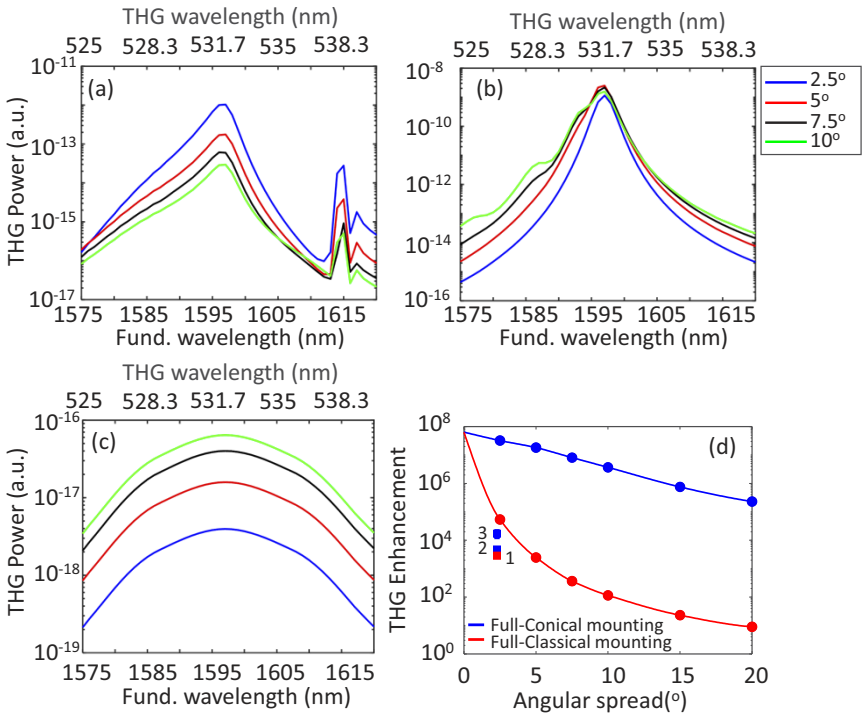

Fig. 3. On-grating THG power for varying angular spread for: (a) full-classical and (b) full-conical mounting conditions. (c) Off-grating THG power for varying angular spread. (d) THG enhancement as a function of varying angular spread. The circular markers correspond to simulated data and solid lines represent the fit. Blue and red curves represent the full-conical and full-classical conditions respectively. Experimental THG enhancements shown as square markers are labelled 1,2,3 corresponding to the no-aperture and rectangular apertures used for angular excitation across $0.86 \times 2.3°$ and $0.43 \times 2.3°$ respectively.

used for the nonlinear optical studies is inherently tied to the angular sensitivity of the GMR, the spatial extent of the grating structures, and the excitation source spectrum utilized. For the present experimental THG studies, the maximum excitation angular span for the standard excitation is limited to ~2.3°, which results in the resonance feature spanning ~20–30 nm in spectral width. This results in a good matching of the resonance feature with the excitation source spectrum. For realizing conical mounting excitation, the angular span along the grating vector direction is reduced from ~2.3° to 0.86° and 0.43° to go from the standard Gaussian-beam like excitation to conical mounting, as discussed below.

3. Experimental studies

The GMR structures were fabricated by depositing 200 nm SiO_2 using plasma enhanced chemical vapor deposition (PECVD) on a 500 µm thick borosilicate-glass substrate. SiO_2 gratings of depth 70 nm were patterned by electron beam lithography and etched using reactive ion etching to fabricate sub-wavelength gratings of pitch (Λ) = 1054 nm and duty cycle = 50%. The gratings were subsequently covered with overlayers of 160 nm SiN and 10 nm a-Si using PECVD. The top-view scanning electron microscopy (SEM) image of the fabricated gratings and corresponding atomic force microscopy (AFM) images are shown in Fig. 4(a) and (b) respectively.

Linear transmission measurements were performed on the fabricated GMR structures of size 1×1 mm^2 using an UV-Vis-NIR spectrometer (Shimadzu MPC3600) with a polarizer placed in

OPTICS CONTINUUM

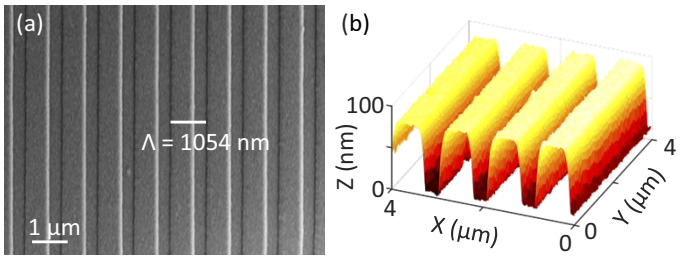

Fig. 4. (a) Scanning Electron Microscopy image and (b) 3D AFM profile of the fabricated gratings.

the path to selectively excite with TE polarized light and an aperture to limit the illumination area. The angular spread of the incident light in the UV-VIS-NIR spectrometer is estimated to be ~1°. The sample was mounted on a rotating stage to change the angle of the grating plane with respect to the incident beam. For studying the AOI dependence under classical and conical mounting condition, the sample was tilted about the x and y-axis respectively. Figures 5(a-d) show the experimentally measured and simulated angular dependence of the transmission spectra for classical and conical mounting conditions. The resonance remains unaltered for conical mounting, whereas for classical mounting the resonance splits into two and moves apart with increasing AOI. The simulated transmission spectra are plotted considering 1° angular spread. The simulation results show good agreement with the experimental spectra, with the resonance wavelength exhibiting splitting/ spectral shifts or remaining almost unchanged with increasing AOI under classical or conical mounting respectively. The quality factors for experimentally measured resonances at normal incidence are estimated to be 79 and 64 whereas the quality factor of the simulated resonances at normal incidence is estimated to be 203 and 391 for full-classical and full-conical mounting respectively. The experimentally measured resonance spectra are found to be wider and hence of lower quality factor. This is attributed to the non-zero angular spread along the non-mounting directions and fabrication imperfections due to etched side-wall roughness, and film non-uniformity.

THG studies were performed using a nonlinear optical microscopy setup as shown in Fig. 6(a). An optical parametric oscillator (OPO) tuned across a wavelength range of 1540–1650 nm with 200 fs pulse-width and 80 MHz repetition rate was used as the fundamental excitation focused on to the sample using a 2x/0.06 numerical aperture (NA) objective. The entrance pupil diameter of the objective lens of 12 mm diameter was partially illuminated with 8 mm diameter incident excitation, resulting in focused incident excitation with an angular spread of ~2.3°. The forward propagating THG signal was collected using a long-working distance condenser lens with 0.5 NA and detected using a photomultiplier tube (PMT) with spectral selectivity achieved using two 900 nm short-pass and one 520+/−60 nm band-pass filters. The condenser lens collected the zeroth and $+1/-1^{th}$ diffraction order THG signals, while $+/-2^{th}$ diffraction order undergoes total internal reflection (TIR) at the glass/air interface. THG images were obtained scanning the GMR device mounted on a motorized stage and mapping the THG signal at every point. Figure 6(b) shows a THG image of the GMR structure obtained close to the resonance wavelength of 1590 nm obtained at an average incident optical power of ~10 mW at the GMR surface. Good spatial contrast is observed across the image with strong nonlinear signal obtained from the GMR structure when compared to the outside region. The THG signal is attributed mainly to the a-Si overlayer, which is verified by ~20-times decrease in THG in the absence of the a-Si layer [25]. Figure 6(c) shows the power dependence of the nonlinear signal as a function of increasing fundamental incident power on the sample. The slope of the plot shown in log-log scale is

OPTICS CONTINUUM

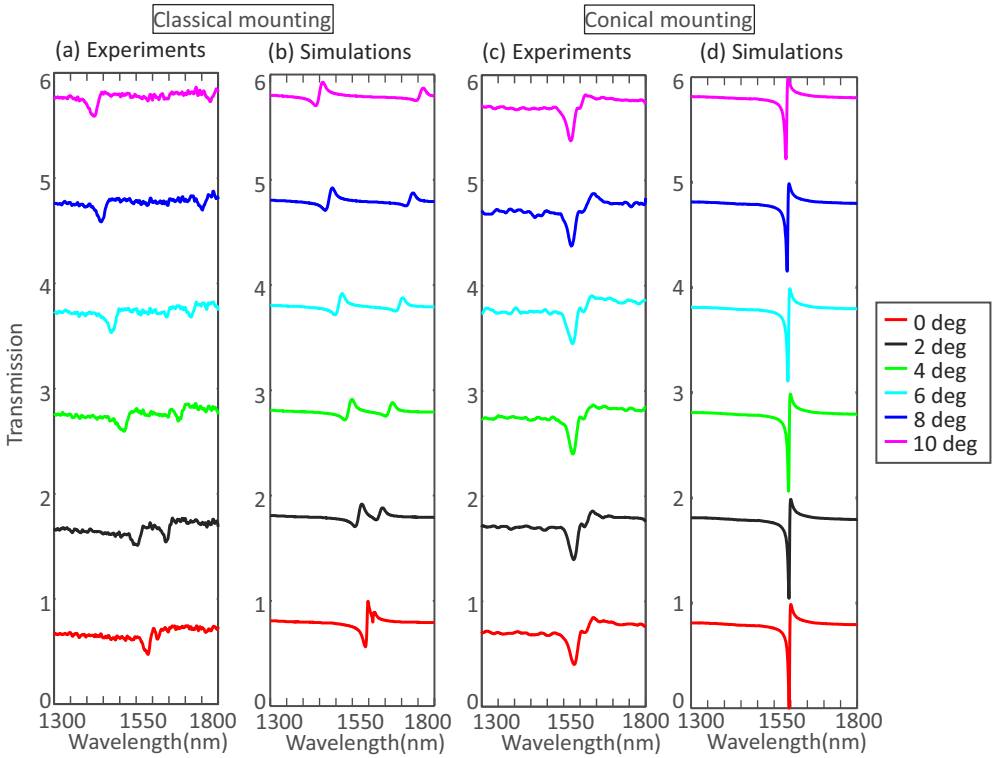

Fig. 5. Angular dependence of experimental and simulated transmission spectra for: (a-b) classical and (c-d) conical mounting conditions. The transmission spectra for increasing AOI are offset by 1-unit along the y-axis for clarity.

obtained as 2.978, confirming that the studied process is a third-order harmonic generation process.

Conical mounting is implemented in this study by inserting a rectangular aperture close to the back-focal plane of the objective lens (denoted by A in Fig. 6(a)). Rectangular apertures of size 3×13 mm and 1.5×13 mm were used to restrict the excitation angles to 0.86°x2.3° and 0.43°x2.3° respectively. With the reduction in excitation angle along the grating vector direction, the illumination resembles the full-conical mounting condition. Figures 7(a-c) show the THG enhancement spectra as a function of fundamental and THG wavelengths for no aperture, 0.86°x2.3° and 0.43°x2.3° angular excitation respectively. The THG enhancement spectra were obtained by taking the ratio of THG signals on and off the GMR structures averaged across 64×64 pixel images. The THG images for the enhancement studies were obtained at an average power of ~10, 21 and 37 mW at the GMR surface for the no aperture and two different aperture settings respectively. The peak on-resonance THG enhancement increases from 2860 to 4740 and 1.7×10^4 for the three cases in the above order. The THG conversion efficiencies for the smallest rectangular aperture was calculated to be $2.53 \times 10^{-6}/\mathrm{W}^2$. Figures 7(d-g) show the THG images on-resonance in the presence of the two different rectangular back-apertures for the rectangular aperture placed parallel (0°) and perpendicular (90°) to the grating lines. Rotation of the rectangular apertures decreases the THG signal thereby confirming that the increase in THG enhancement can be unambiguously attributed to the GMR structure excited under conical mounting condition. The rectangular aperture placed at 0° and 90° corresponds to conical and classical mounting conditions respectively. The experimentally measured THG signal ratio for

OPTICS CONTINUUM

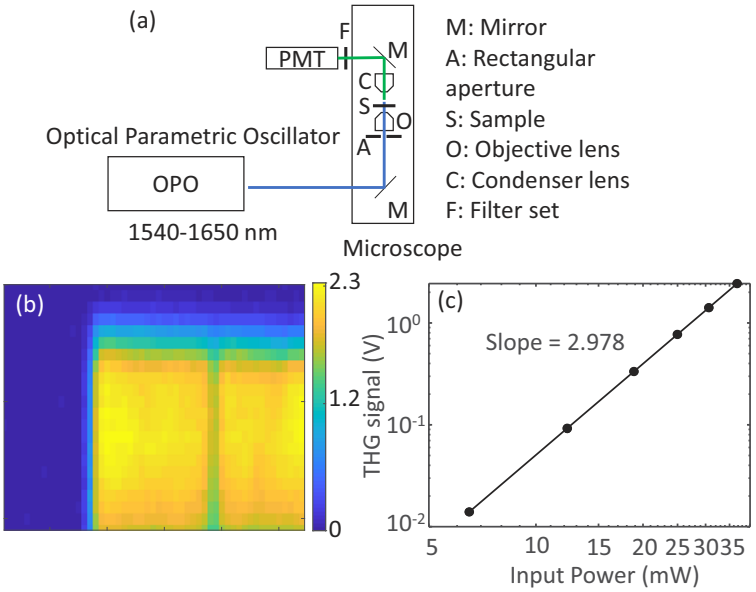

Fig. 6. (a) Schematic of the nonlinear microscopy setup used for THG study. (b) THG image of the GMR structure at resonance wavelength of 1590 nm in absence of rectangular pupil mask. (c) Power dependence plot of the THG signal as a function of fundamental incident power.

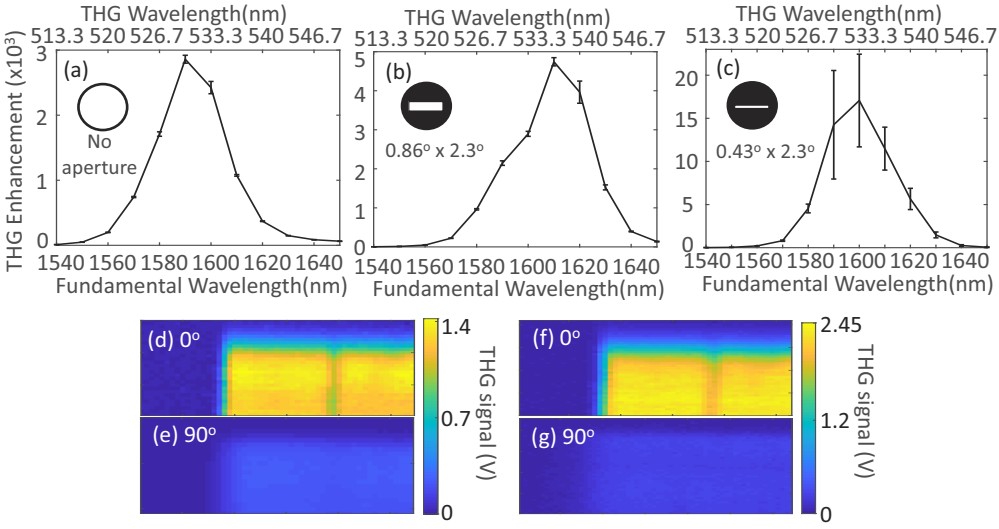

Fig. 7. Enhancement spectra considering (a) no aperture and rectangular pupil masks with angular spread of: (b) 0.86°x2.3° and (c) 0.43°x2.3°. Representation of the rectangular pupil mask used in each case is shown as inset. THG images at the respective resonance wavelengths are shown in (d-e) for 0.86°x2.3° and (f-g) 0.43°x2.3° angular spread respectively. Bottom figures (e) and (g) show the THG images when the rectangular pupil masks are rotated by 90°.

OPTICS CONTINUUM

the conical and classical mounting cases are obtained as 5.35 and 8.46 for the two rectangular apertures used. This points to the improvement in THG signal ratio for the conical mounting with reduced angular excitation along the grating vector direction. The maximum THG enhancements obtained in the experimental work are also shown in Fig. 3(d) for comparison with the simulation studies (filled rectangles labelled 1, 2 and 3). The reduced THG enhancement observed in the experiments when compared to the simulations is attributed to full-conical and full-classical mounting condition used in the simulations which differs from the actual experiments with the apertures restricting the angular spread along the grating vector but not eliminate it.

4. Conclusions

In conclusion, THG enhancement from ultra-thin a-Si layer deposited on SiN GMR structures using conical mounting through pupil-function engineered fundamental excitation is reported. The forward detected THG enhancement is found to improve from 2860 for no aperture case to 4740 and 1.7×10^4 from an a-Si layer utilizing rectangular masks of size 3×13 mm (angular spread: 0.86°x2.3°) and 1.5×13 mm (angular spread: 0.43°x2.3°) respectively placed in the back-focal plane of the focusing optics. This improvement in THG enhancement is attributed to reduced angular sensitivity of the GMR resonances under conical mounting when compared to classical mounting condition. It is useful to compare the THG enhancements achieved in this work with some notable reports of THG enhancement from silicon-based resonant metasurfaces. This includes, ~500-times enhancement from 220–260 nm thick nanodisks supporting magnetic dipole resonances [8], 1.5×10^5 enhancement from 120 nm nanodisk-bar structures supporting electromagnetically induced transparency-like resonances [16], 10^5 enhancement from 500 nm high quality factor quasi-bound state in continuum resonances [19], and 500-times enhancement from 53 nm thick asymmetric holey-disk structures [38]. In comparison to these previous THG studies, the present work makes use of a-Si nonlinear medium of only 10 nm to achieve more than four-orders of magnitude enhancement in THG. The use of conical mounting is a promising approach to enhance nonlinear optical processes from angle sensitive GMR structures. The experimental demonstration in this paper is focused on a specific implementation of silicon based multilayer GMR structure with large angular sensitivity. Nonetheless, the technique presented in this work is a general approach to enhance nonlinear optical processes by suitably selecting the excitation angular span for conical mounting based on the angular sensitivity of the GMR structure or resonant metasurface.

Funding. Department of Science and Technology, Ministry of Science and Technology, India (QUST programme); Science and Engineering Research Board (Core Research Grant); Ministry of Electronics and Information technology (NNetra); Nano Mission Council (NNetra).

Acknowledgement. The authors acknowledge the National Nanofabrication Centre and Micro-Nano Characterization Facility at Indian Institute of Science, Bangalore for allowing to carry out the fabrication and characterization studies presented in this work.

Disclosures. The authors declare no conflicts of interest.

Data availability. Data underlying the results presented in this paper are not publicly available at this time but may be obtained from the authors upon reasonable request.

References

1. Z. S. Liu, S. Tibuleac, D. Shin, P. P. Young, and R. Magnusson, "High-efficiency guided-mode resonance filter," Opt. Lett. **23**(19), 1556–1558 (1998).
2. G. Pitruzzello and T. F. Krauss, "Photonic crystal resonances for sensing and imaging," J. Opt. **20**(7), 073004 (2018).
3. P. K. Sahoo, S. Sarkar, and J. Joseph, "High sensitivity guided-mode-resonance optical sensor employing phase detection," Sci Rep **7**(1), 1–7 (2017).
4. B. T. Cunningham, "Photonic crystal surfaces as a general purpose platform for label-free and fluorescent assays," JALA-J. Lab. Autom. **15**(2), 120–135 (2010).
5. S. H. G. Menon, A. S. Lal Krishna, and V. Raghunathan, "Silicon nitride based medium contrast gratings for doubly resonant fluorescence enhancement," IEEE Photonics J. **11**(4), 1–11 (2019).

OPTICS CONTINUUM

6. T. Ning, H. Pietarinen, O. Hyvärinen, R. Kumar, T. Kaplas, M. Kauranen, and G. Genty, "Efficient second-harmonic generation in silicon nitride resonant waveguide gratings," Opt. Lett. **37**(20), 4269–4271 (2012).
7. J. H. Lin, C. Y. Tseng, C. T. Lee, J. F. Young, H. C. Kan, and C. C. Hsu, "Strong guided mode resonant local field enhanced visible harmonic generation in an azo-polymer resonant waveguide grating," Opt. Express **22**(3), 2790–2797 (2014).
8. M. R. Shcherbakov, D. N. Neshev, B. Hopkins, A. S. Shorokhov, I. Staude, E. V. Melik-Gaykazyan, M. Decker, A. A. Ezhov, A. E. Miroshnichenko, I. Brener, A. A. Fedyanin, and Y. S. Kivshar, "Enhanced third-harmonic generation in silicon nanoparticles driven by magnetic response," Nano Lett. **14**(11), 6488–6492 (2014).
9. S. Liu, M. B. Sinclair, S. Saravi, G. A. Keeler, Y. Yang, J. Reno, G. M. Peake, F. Setzpfandt, I. Staude, T. Pertsch, and I. Brener, "Resonantly Enhanced second-harmonic generation using III–V semiconductor all-dielectric metasurfaces," Nano Lett. **16**(9), 5426–5432 (2016).
10. J. Deka, K. K. Jha, S. Menon, A. S. Lal Krishna, R. Biswas, and V. Raghunathan, "Microscopic study of resonant third-harmonic generation from amorphous silicon nanodisk arrays," Opt. Lett. **43**(21), 5242–5245 (2018).
11. R. Biswas, J. Deka, K. K. Jha, V. Praveen, A. S. Lal Krishna, S. Menon, and V. Raghunathan, "Resonant four-wave mixing microscopy on silicon-on-insulator based zero-contrast gratings," OSA Continuum **2**(10), 2864–2874 (2019).
12. K. I. Okhlopkov, A. Zilli, A. Tognazzi, D. Rocco, L. Fagiani, E. Mafakheri, M. Bollani, M. Finazzi, M. Celebrano, M. R. Shcherbakov, C. De Angelis, and A. A. Fedyanin, "Tailoring third-harmonic diffraction efficiency by hybrid modes in high-Q metasurfaces," Nano Lett. **21**(24), 10438–10445 (2021).
13. S. S. Wang and R. Magnusson, "Theory and applications of guided-mode resonance filters," Appl. Opt. **32**(14), 2606–2613 (1993).
14. C. J. Chang-Hasnain and W. Yang, "High-contrast gratings for integrated optoelectronics," Adv. Opt. Photonics **4**(3), 379–440 (2012).
15. A. S. Lal Krishna, V. Mere, S. K. Selvaraja, and V. Raghunathan, "Polarization-independent angle-tolerant mid-infrared spectral resonance using amorphous germanium high contrast gratings for notch filtering application," OSA Continuum **3**(5), 1194–1203 (2020).
16. Y. Yang, W. Wang, A. Boulesbaa, I. I. Kravchenko, D. P. Briggs, A. Puretzky, D. Geohegan, and J. Valentine, "Nonlinear Fano-resonant dielectric metasurfaces," Nano Lett. **15**(11), 7388–7393 (2015).
17. K. Koshelev, S. Lepeshov, M. Liu, A. Bogdanov, and Y. Kivshar, "Asymmetric metasurfaces with high-Q resonances governed by bound states in the continuum," Phys. Rev. Lett. **121**(19), 193903 (2018).
18. J. Jeong, M. D. Goldflam, S. Campione, J.L. Briscoe, P.P. Vabishchevich, J. Nogan, M.B. Sinclair, T.S. Luk, and I. Brener, "High quality factor toroidal resonances in dielectric metasurfaces," ACS Photonics **7**, 1699–1707 (2020).
19. Z. Liu, Y. Xu, Y. Lin, J. Xiang, T. Feng, Q. Cao, J. Li, S. Lan, and J. Liu, "High-Q quasibound states in the continuum for nonlinear metasurfaces," Phys. Rev. Lett. **123**(25), 253901 (2019).
20. T. Sun, W. Yang, and C. Chang-Hasnain, "Surface-normal coupled four-wave mixing in a high contrast gratings resonator," Opt. Express **23**(23), 29565–29572 (2015).
21. Z. Liu, J. Wang, B. Chen, Y. Wei, W. Liu, and J. Liu, "Giant enhancement of continuous wave second harmonic generation from few-layer GaSe Coupled to high-Q quasi bound states in the continuum," Nano Lett. **21**(17), 7405–7410 (2021).
22. R. Magnusson, "Wideband reflectors with zero-contrast gratings," Opt. Lett. **39**(15), 4337–4340 (2014).
23. M. J. Uddin and R. Magnusson, "Efficient guided-mode-resonant tunable color filters," IEEE Photon. Technol. Lett. **24**(17), 1552–1554 (2012).
24. J. M. Bendickson, E. N. Glytsis, T. K. Gaylord, and D. L. Brundrett, "Guided-mode resonant subwavelength gratings: effects of finite beams and finite gratings," J. Opt. Soc. Am. A **18**(8), 1912–1928 (2001).
25. S. Menon, A. Prosad, A. S. Lal Krishna, R. Biswas, and V. Raghunathan, "Resonant mode engineering in silicon compatible multilayer guided-mode resonance structures under Gaussian beam excitation condition," J. Opt. **23**(10), 105001 (2021).
26. T. Ning, X. Li, Y. Zhao, L. Yin, Y. Huo, L. Zhao, and Q. Yue, "Giant enhancement of harmonic generation in all-dielectric resonant waveguide gratings of quasi-bound states in the continuum," Opt. Express **28**(23), 34024–34034 (2020).
27. N. V. Proscia, Z. Shotan, H. Jayakumar, P. Reddy, C. Cohen, M. Dollar, A. Alkauskas, M. Doherty, C. A. Meriles, and V. M. Menon, "Near-deterministic activation of room-temperature quantum emitters in hexagonal boron nitride," Optica **5**(9), 1128–1134 (2018).
28. D. Lacour, G. Granet, and J.-P. Plumey, "Polarization independence of a one-dimensional grating in conical mounting," J. Opt. Soc. Am. A **20**(8), 1546–1552 (2003).
29. Y.-H. Ko, M. Niraula, and R. Magnusson, "Divergence-tolerant resonant bandpass filters," Opt. Lett. **41**(14), 3305–3308 (2016).
30. R. Magnusson and Y-H. Ko, "Guided-mode resonance nanophotonics: fundamentals and applications," Proc. SPIE **9927**, 992702 (2016).
31. N. Saha and W. Kou, "Guided-mode resonance-based bandpass filter operating at full conical mounting," Appl. Opt. **59**(34), 10700–10705 (2020).
32. R. Yukino, P. K. Sahoo, J. Sharma, T. Takamura, J. Joseph, and A. Sandhu, "Wide wavelength range tunable one-dimensional silicon nitride nano-grating guided mode resonance filter based on azimuthal rotation," AIP Adv. **7**(1), 015313 (2017).

OPTICS CONTINUUM

33. P. K. Sahoo, J. Sharma, R. Yukino, A. Sandhu, and J. Joseph, "High azimuthal angle tolerant dual-channel wavelength filter from visible to NIR using conically mounted guided mode resonance structures," Opt. Lett. **45**(21), 6010–6013 (2020).
34. W. L. Chen, K. D. Long, H. J. Yu, Y. F. Tan, J. S. Choi, B. A. Harley, and B. T. Cunningham, "Enhanced live cell imaging via photonic crystal enhanced fluorescence microscopy," Analyst **139**(22), 5954–5963 (2014).
35. V. Liu and S. Fan, "S4: a free electromagnetic solver for layered periodic structures," Comput. Phys. Commun. **183**(10), 2233–2244 (2012).
36. COMSOL Multiphysics, Wave Optics Module User's Guide, COMSOL AB, Stockholm, Sweden (2019), https://doc.comsol.com/5.5/doc/com.comsol.help.woptics/IntroductionToWaveOpticsModule.pdf
37. R.W. Boyd, *Nonlinear Optics* (Academic, 2020).
38. L. Xu, K. Z. Kamali, L. Huang, M. Rahmani, A. Smirnov, R. Camacho-Morales, Y. Ma, G. Zhang, M. Woolley, D. Neshev, and A. E. Miroshnichenko, "Dynamic nonlinear image tuning through magnetic dipole quasi-BIC ultrathin resonators," Adv. Sci. **6**(15), 1802119 (2019).